Band-gap modulation of two-dimensional saturable absorbers for solid-state lasers

Shuxian Wang,[1] Haohai Yu,[1,2] and Huaijin Zhang[1,3]

[1]*State Key Laboratory of Crystal Materials and Institute of Crystal Materials, Shandong University, Jinan 250100, China*
[2]*e-mail: haohaiyu@sdu.edu.cn*
[3]*e-mail:huaijinzhang@sdu.edu.cn*

Received December 24, 2014; revised February 10, 2015; accepted February 12, 2015;
posted February 13, 2015 (Doc. ID 231453); published March 16, 2015

Due to the manifestation of fascinating physical phenomena and materials science, two-dimensional (2D) materials have recently attracted enormous research interest with respect to the fields of electronics and optoelectronics. There have been in-depth investigations of the nonlinear properties with respect to saturable absorption, and many 2D materials show potential application in optical switches for passive pulsed lasers. However, the Eigen band-gap determines the responding wavelength band and constrains the applications. In this paper, based on band-gap engineering, some different types of 2D broadband saturable absorbers are reviewed in detail, including molybdenum disulfide (MoS_2), vanadium dioxide (VO_2), graphene, and the Bi_2Se_3 topological insulator. The results suggest that the band-gap modification should play important roles in 2D broadband saturable materials and can provide some inspiration for the exploration and design of 2D nanodevices.

OCIS codes: (140.0140) Lasers and laser optics; (140.3540) Lasers, Q-switched; (140.3380) Laser materials; (140.3538) Lasers, pulsed.
http://dx.doi.org/10.1364/PRJ.3.000A10

1. INTRODUCTION

Lasers, since first demonstrated by a ruby crystal in 1960 [1], have shown tremendous progress so far. On account of the advantages of large pulse energy, short pulse duration, and high peak power, pulse lasers, including mode-locking and *Q*-switching, receive more widespread attention [2,3]. Pulsed lasers with the pulse width from nanosecond to subpicosecond scales play a key role in the industrial machining, remote sensing, and military defense areas [4]. Ultrashort femtosecond lasers have significant applications in the fields of the in-situ detection, complex reaction dynamics, medical survey, and telecommunication [3]. Passive pulse modulation could be operated with compact and cost-effective structures, such that it has become an influential research direction in the laser field. Taking advantage of saturable absorption of saturable absorbers, that is part of the third-order nonlinear properties, passive pulse modulation in the *Q*-switched or mode-locking lasers could be easily implemented. Traditional saturable absorbers, such as ion-doped crystals (Cr:YAG, Cr:ZnSe, V:YAG, and so on) [5–7], GaAs [8], and color-center crystals (for example F_2:LiF) [9], are wavelength-sensitive and are only applied in their respective corresponding wavelength bands. Although the commercial semiconductor saturable absorber mirrors (SESAMs) could be fabricated for the specific wavelength from 0.4 to 2.5 μm by using different semiconductor material systems [2,10], the relatively complex structural design may increase the product cost and the difficulty of preparation. In addition, the quasi-phase-matching technique in optical superlattice, which is feasible for a wide wavelength range as long as it is in the transparent spectral region of the optical superlattice material, is also a promising method to obtain passive mode-locking lasers [11–13]. Nevertheless, this technique requires the high-efficiency generation of second-harmonic generation and elaborate design of the resonant cavity and the second-harmonic crystal. Therefore, the development of low-cost and robust broadband saturable absorbers is still an intense focus of research nowadays [2].

Graphene, as the representative of the two-dimensional (2D) materials, since found by K. Geim and K. S. Novoselov, has profoundly promoted and broadened the research areas of 2D materials in the fields of electronics and optoelectronics due to an abundance of fantastic physics [14–23]. With in-depth studies, many other novel 2D materials are discovered and are brought into people's horizons, such as transition metal dichalcogenides (TMDCs) (typically MoS_2, $MoSe_2$, WS_2, and so on) [16,17,19,24,25], transition metal oxides (for instance MoO_3 and TiO_2) [17,24,26], topological insulators (Bi_2Se_3, Bi_2Te_3, and Sb_2Te_3) [16,17,24,27], as well as silicone [28], germanane [16,28], black phosphorus [29,30], and other graphene analogues (typically *h*-BN) [19,24]. For the major 2D materials, the layered structure results in the strong in-plane coupling and the weak van der Waals coupling between layers. Therefore monolayer or few-layer 2D perfect samples could be easily fabricated by mechanical exfoliation or chemical exfoliation [18,31]. In addition, aiming at the growth habits and atomic arrangements for different 2D materials, many more efforts are made to explore the economical and practical growth methods, such as chemical vapor deposition, and epitaxial growth on adaptive substrates [21,25]. The layered 2D materials exhibit numerous exotic physical, chemical, and mechanical properties such that they are rapidly developed. Many potential functional applications in terms of 2D materials in some aspects will be realized in the near future,

including optical modulators, photodetectors, logic transistors, high-frequency transistors, energy storage, and sensor devices [16–18,24,31].

Most 2D semiconductor materials show a simple two energy band structure of the conduction band and the valence band. Light that is of higher energy than the gap energy can excite carriers from the valance band to the conduction band. If the excitation has stronger intensity, all possible initial states are depleted and the final states are partially occupied in accordance with the Pauli blocking effect such that the absorption will be saturated [2]. Thus the 2D semiconductor materials give some opportunities for the fabrication of cost-effective and flexible broadband saturable absorbers, and some 2D materials have realized this goal [4,32–34]. Saturable absorption is the modulation of nonlinear absorption. However, the bandgap of a semiconductor determines the responding wavelength and every semiconductor has its specialized bandgap. Based on the photoelectric effect, the semiconductors materials with a narrow bandgap have broad responding wavelength bands. Therefore, besides the narrow bandgap, for 2D materials such as graphene, the modulation of the bandgap should be important, especially for the materials with large bandgaps such as MoS_2 [13,35]. In this review, what is discussed will mainly concentrate on the state-of-the-art research exploration and development about the saturable absorbers for several 2D materials. The content consists of the band-gap modification by impurity of MoS_2, band-gap modulation by phase transition of VO_2, and broadband modulation by inherent bandgaps for graphene and Bi_2Se_3 topological insulator. This work can show some guiding designing functions for the investigation of other 2D layered optoelectronic materials.

2. BAND-GAP ENGINEERING FOR MoS_2

Layered MoS_2, a typical representative of the layered TMDCs family, is composed of the sandwiches combined by van der Waals interactions, and each sandwich consists of covalently bound S–Mo–S trilayers with two hexagonal layers of S atoms and an intermediate hexagonal plane of Mo atoms [17,25,36–38]. The monolayer MoS_2 has a direct band-gap at the K point of the Brillouin zone with a gap of 1.8 eV (0.7 μm), and the bulk MoS_2 is of an indirect band-gap between the Γ point (valence band) and K point (conduction band) of the Brillouin zone with a gap of ranging from 0.86 eV (1.4 μm) to 1.29 eV (1.0 μm) [39–44]. Besides the change of thickness, the bandgap of MoS_2 was also modified by the other engineering technologies, such as the external electric field and the external strain [45–48]. Atomic-layered MoS_2 exhibits intriguing physical properties distinct from its bulk state, for example, the dramatical increasing of luminescence quantum efficiency for MoS_2 from the bulk state to single layer. Therefore, layered MoS_2 attracts more interest in the fabrication of ultrathin and flexible nanoelectronic devices [16,25], and was brought into various research fields, such as lubrication, hydrodesulfurization catalysis, supercapacitors, and field-effect transistors [36–38,49].

Monolayer MoS_2 has been proven with strong optical response, such as enhanced photon absorption and large photocurrent caused by van Hove singularities or band nesting [50,51]. In 2012, using the spatially and temporally resolved pump-probe technique with a 390 nm pump source and a 660 nm probe source, R. Wang *et al.* measured and discussed the ultrafast carrier dynamics of atomically thin MoS_2 [52]. One year later, more nonlinear investigations were carried out [53–55], and it is significant that ultrafast saturable absorption of MoS_2 nanosheets was demonstrated around 800 nm by K. P. Wang *et al.* [56].

Most of the studies were in pursuit of the high-quality layered MoS_2 samples in order to obtain remarkable electronic and optical properties [37–39]; however, the generation of defects, which deviate from a perfect crystal structure, was inevitable in the preparation of MoS_2 samples. The probable defects could localize electronic states and change the energy level, leading to some fantastic physical phenomena, such as the Mott transition and Anderson localization [57].

Recently, S. X. Wang *et al.* systematically analyzed the band-gap change of multilayer MoS_2 in a theoretical analysis with the ratio (R) between Mo and S atoms slightly deviating from 1:2 [34]. The first-principle theoretical calculations were performed by using the plane-wave basis Vienna *ab initio* simulation package [58,59], and the atomic arrangement of MoS_2 was the universal AB stacking (2H – MoS_2). As shown in Fig. 1, the bandgap is about 1.08 eV (1.2 μm) for multilayered MoS_2 with the stoichiometric ratio, which corresponds well to the previous calculated value for bulk MoS_2 [40]. The other results with different R values are displayed in Fig. 2. When R is larger than 2.09, MoS_2 exhibits metallic character, and the generation of saturable absorption requiring suitable patterns or distances between the metal units becomes difficult. When the R is located in the range 1.89–2 and 2–2.09, few-layered MoS_2 showed an indirect semiconductor property and its energy gap is 0.08 eV (15.5 μm), 0.23 eV (5.4 μm), 0.48 eV (2.6 μm), 0.63 eV (2.0 μm), and 0.26 eV (4.7 μm) for the R with a value of 2.09, 2.04, 1.97, 1.94, and 1.89, respectively. Thus, it can be concluded that the band-gap of MoS_2 would be reduced by the introduction of some Mo or S defects in a suitable range. The smaller band-gap means the broadband saturable absorption of defective MoS_2 becomes possible.

Then the MoS_2 samples were fabricated by the pulse laser deposition (PLD) method, which is an efficient technique to produce the S imperfections for MoS_2 samples, since low-mass S is evaporated more easily than high-mass Mo [60]. The R lies in the range 1.89–1.97 moving from the center to the edge of the sample surveyed by X-ray photoelectron spectrometry. As demonstrated in Fig. 3, the measured absorbance of the MoS_2 sample decreases with an increase of wavelength [34]. For the R with the value of 1.89, the energy gap for MoS_2 samples is only 0.26 eV, corresponding to a wavelength of 4.7 μm. In contrast to the absorption range of standard

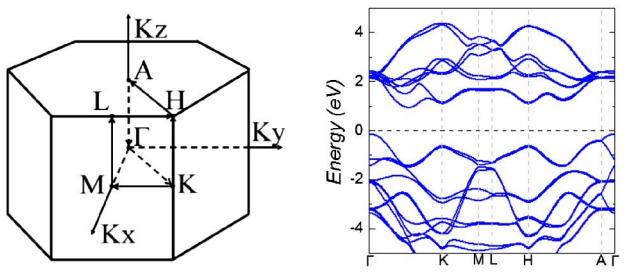

Fig. 1. Brillouin zone (left) and calculated band structure (blue lines, right) of bulk MoS_2 with stoichiometric ratio. Selected from Ref. [34].

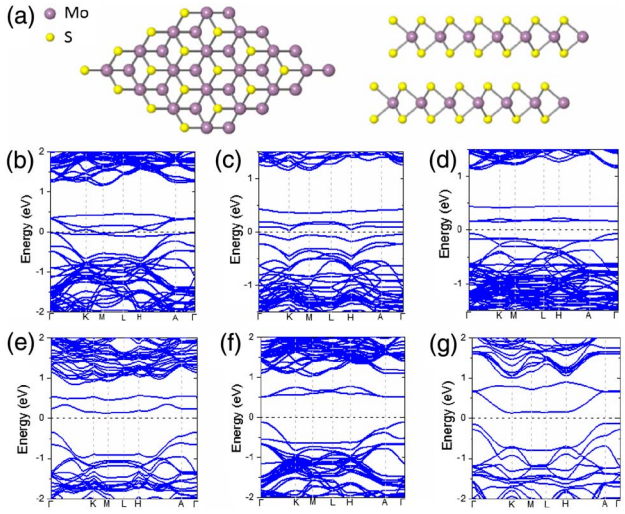

Fig. 2. Theoretical band gap of MoS_2 samples; (a) AB stacked MoS_2 observed from the top (left) and side (right); (b) calculated band structure of bulk MoS_2 with $R = 1{:}2.12$; (c) calculated band structure of bulk MoS_2 with $R = 1{:}2.09$; (d) calculated band structure of bulk MoS_2 with $R = 1{:}2.04$; (e) calculated band structure of bulk MoS_2 with $R = 1{:}1.97$; (f) calculated band structure of bulk MoS_2 with $R = 1{:}1.94$; (g) calculated band structure of bulk MoS_2 with $R = 1{:}1.89$. Selected from Ref. [34].

stoichiometric MoS_2, the prepared MoS_2 samples are more likely to have broadband saturable absorption.

Saturable absorption of MoS_2 was investigated employing the two-level saturable absorber model widely used for 2D quantum wells [61,62]

$$\alpha^* = \frac{\alpha_S^*}{1 + \frac{N}{N_S}} + \alpha_{\mathrm{NS}}^*, \tag{1}$$

$$N = \frac{\alpha^* I \tau}{\hbar \omega}, \tag{2}$$

where $\alpha^*(N)$ is the absorption coefficient, and α_S^* and α_{NS}^* are the saturable and nonsaturable absorption coefficient, respectively. N is the photoinduced electron hole density, and N_S, the saturation density, is the value of N for which the absorption falls to one-half of its initial value. I is the incident light intensity of a continuous-wave (cw) or long-pulse excitation source, τ is the carrier recombination time, and ω is the light frequency. Combined with the Eqs. (1) and (2), the saturable absorption equation can therefore be expressed as [32,61]

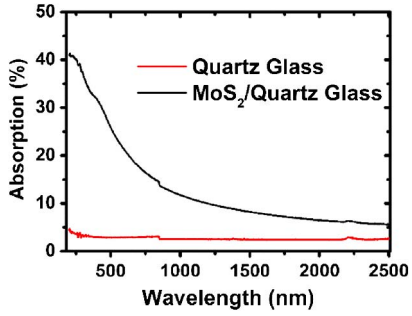

Fig. 3. Measured absorption spectrum of MoS_2 sample. Selected from Ref. [34].

$$\alpha^* = \frac{\alpha_S^*}{1 + \frac{I}{I_S}} + \alpha_{\mathrm{NS}}^*, \tag{3}$$

where the saturation intensity I_S is a most important parameter to describe how easy or difficult that the photoinduced electron hole pairs are fully saturated in the saturable absorption process. With the exponential relationship between absorption and transmission, the power-dependent nonlinear transmittance T could be fitted with the following [63,64]

$$T = A \exp\left(\frac{-\delta T}{1 + \frac{I}{I_S}}\right), \tag{4}$$

where T is the transmission, A is a normalization constant, and δT is the absolute modulation depth.

Saturable absorption of the as-grown MoS_2 sample was measured with a picosecond pulse laser with a pulse width of 40 ps at 1.06 μm, and the data was analyzed with Eq. (4). The saturation intensity of MoS_2 was calculated with 2.45 GW/cm^2, a value larger than that of graphene (0.61–0.71 MW/cm^2) and comparable to that of Bi_2Se_3 (4.3 GW/cm^2). The saturable carrier density N_s is about 1.4×10^{17} cm^{-2}, a magnitude 2–3 orders larger than graphene (5.84×10^{13} to 8.16×10^{14} cm^{-2}) [32,34,63].

Using the MoS_2 samples as saturable absorbers, passively Q-switched lasers at wavelengths of 1.06, 1.42, and 2.1 μm were successfully operated with Nd:$GdVO_4$, Nd:$Y_3Ga_5O_{12}$ (Nd:YGG), and Tm:Ho:$Y_3Ga_5O_{12}$ (Tm:Ho:YGG) crystals, respectively, as gain materials. The average output power and the repetition rate with the increase of pump power are demonstrated in Fig. 4, and the typical pulses at the wavelengths of 1.06, 1.42, and 2.1 μm are shown in Fig. 5. Q-switched lasers for the broadband MoS_2 saturable absorber, ranging from 1.06 to 2.1 μm were obtained in this experiment with submicrosecond temporal widths and maximum output powers of up to a few hundred milliwatts.

Many research results about the pulse modulation with MoS_2 saturable absorbers have been demonstrated so far. It has shown remarkable mode-locking or Q-switched

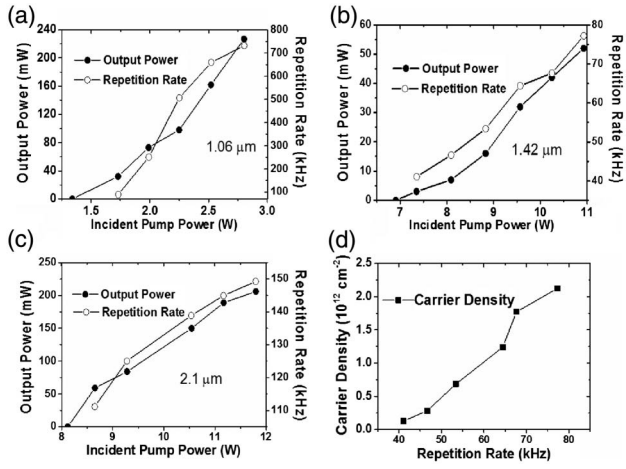

Fig. 4. Average output power and repetition rate of passively Q-switched laser; (a) passively Q-switched Nd:$GdVO_4$ laser performance at 1.06 μm; (b) passively Q-switched Nd:YGG laser performance at 1.42 μm; (c) passively Q-switched Tm:Ho:YGG laser performance at 2.1 μm; (d) relation between the carrier density (N) and pulse repetition rate at the laser wavelength of 1.42 μm. Selected from Ref. [34].

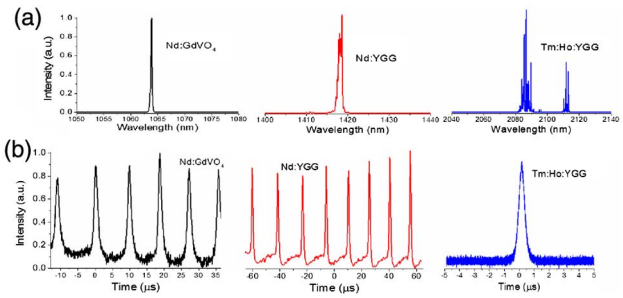

Fig. 5. Passively Q-switched laser spectra and pulses; (a) passively Q-switched Nd:$GdVO_4$, Nd:YGG, and Tm:Ho:YGG laser spectra of at center wavelengths of 1.06, 1.42, and 2.1 μm, respectively; (b) passively Q-switched Nd:$GdVO_4$, Nd:YGG, and Tm:Ho:YGG laser spectra with the pulse width of 970, 729, and 410 ns, respectively. Selected from Ref. [34].

performance in the different gain materials, such as Yb-doped fibers (around 1 μm) [65,66], Er-doped fibers (1.5 to 1.6 μm) [67–70], Tm-doped fiber (around 2 μm) [71], Nd:$GdVO_4$ [34], Nd:YGG [34], and Tm:Ho:YGG [34]. For the perfectly single-layered MoS_2, saturable absorption is hardly acquired when the wavelength is above 0.7 μm due to the large band-gap (1.8 eV). Even if MoS_2 is in the bulk state (1.08 eV), the modulation wavelength would still be not longer than 1.2 μm [34]. Employing band-gap engineering, which is similar to the fabrication of SESAMs [13], broadband pulse modulation for few-layer MoS_2 was successfully obtained with a range 1.06–2.1 μm. This approach may benefit the exploitation and development of new 2D optoelectronic devices for some 2D materials with a large inherent band-gap.

3. PHASE-TRANSITION MODULATION FOR VO_2

Phase transitions are ubiquitous in nature, such as superconductive phase transitions [72], ferroelectric and antiferroelectric phase transitions [73], and insulator–metal transitions (IMTs) [74–81]. The complex physical science contained in the transition process is intriguing with respect to the study of phase-transition kinetics in an attempt to well-understand the changes of energy structure, electron correlation, electron-lattice coupling, and so on [79]. VO_2, an archetypal IMT, exhibits a reversible IMT at about 340 K accompanied by a transition from a low-temperature insulating phase with a monoclinic space group of $P2_1/c$ to a high-temperature rutile metallic phase with a tetragonal space group of $P4_2/mnm$ [75,77,79]. Therefore, it worth noting that the IMT phase transition of VO_2 could change the bandgap and broaden the responding wavelength band with the increase of the temperature.

The IMT of VO_2 could be considered as the Coulomb interactions between $3d$ electrons of V^{4+} ions and the degeneracy of their energy levels. For the rutile metallic phase of VO_2, each V^{4+} ion is located at the octahedral site surrounded by six O^{2-} ions. Based on the Goodenough's model [82], the d levels of the V^{4+} ions are first split into low-energy triply degenerate t_{2g} states and high-energy doubly degenerate e_g^σ states. The e_g^σ states lie 3.5 eV above the Fermi level and are empty bands [75,83]. The t_{2g} multiplet then are separated into an a_{1g} singlet ($d_\parallel$ state) and an e_g^π doublet (π state and π^* state). The $a_{1g}(d_\parallel)$ orbitals are parallel to the c-axis with σ bonding of V–V pairs, and the e_g^π doublet (π and π^*) are strongly hybridized with the O $2p$ orbitals. The $d_\parallel$ orbitals and π^* orbitals partly overlap and both of them partially occupy the Fermi level. The monoclinic insulating phase is identified as a Peierls–Mott insulator, and in that phase, the dimerization and tilting of the V–V pairs could lead to the $d_\parallel$ band along the c-axis is split into a lower-energy bonding combination and a higher-energy anti-bonding one ($d_\parallel^*$) [83–85]. Moreover, the e_g^π states (π^* state) are shifted to the upper position because of the increase of hybridization between the e_g^π doublet with O $2p$ orbitals. Ultimately, for the monoclinic phase, the bonding $d_\parallel$ orbitals are completely occupied, but the anti-bonding $d_\parallel(d_\parallel^*)$ and π^* orbitals are empty due to both states being above the Fermi level [78–80,83–85].

IMT of VO_2 could be triggered with different stimuli, such as temperature, light, electric field, mechanical strain, and magnetic field [76–78,86–88]. In terms of linear optical response, VO_2 undergoes a large and rapid change, so it has potential use in ultrafast switching and sensing [89]. However the nonlinear optical response of VO_2 with respect to pulse modulation in the IMT process, which is vital in terms of photonic and optoelectronic applications, has not reported up to now.

Using the first-principle theoretical calculations and the atomic structural parameters previously reported [58,59,80], the density of states (DOSs) for VO_2 in the different states were calculated, consisting of the insulating phase, phases near the IMT point, and metallic phase [90]. As presented in Fig. 6, the room-temperature monoclinic phase behaves as an insulator with a band-gap of 0.68 eV, coinciding well with the result measured by photoemission spectroscopy [83]. In addition, accompanied by the IMT being in progress, the VO_2 band-gap decreases and its phase enters a tetragonal metallic state from the monoclinic insulating state. The calculation of DOS for two phases at the IMT temperature point indicates that VO_2 has an optical response to light with a wavelength shorter than 1.85 μm (0.68 eV), corresponding to the band-gap of the pure insulating phase.

As displayed in Fig. 7, the linear optical response of the VO_2 sample fabricated by the PLD method was investigated at

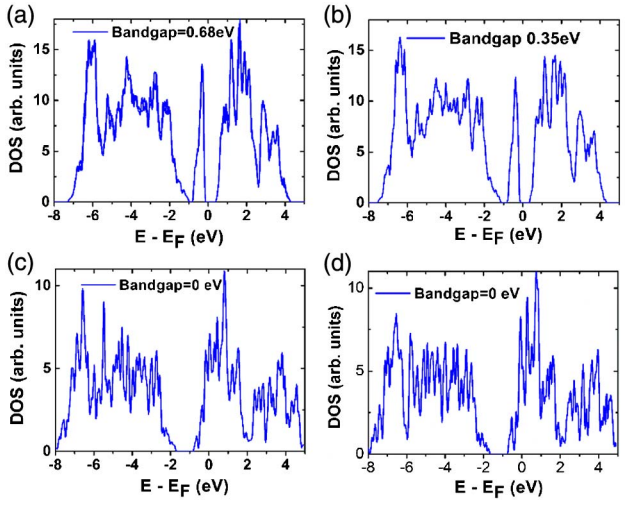

Fig. 6. Theoretical DOS for VO_2 in different phases; (a) DOS in the monoclinic phase at room temperature with a band-gap of 0.68 eV; (b) DOS in the monoclinic phase near the IMT point with a band-gap of 0.36 eV; (c) DOS in the tetragonal phase near the IMT point; (d) DOS in the tetragonal phase and final metallic states. Selected from Ref. [90].

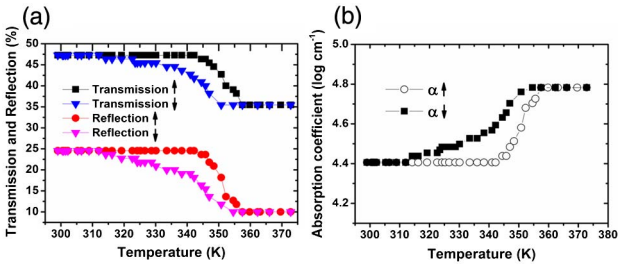

Fig. 7. Linear optical response of VO_2 layer; (a) reflection and transmission of VO_2 at different temperatures and light wavelength of 1.06 μm measured by increasing (↑) and decreasing (↓) the temperature; (b) linear absorption coefficient of VO_2 at different temperatures and light wavelength of 1.06 μm measured by increasing (↑) and decreasing (↓) the temperature. Selected from Ref. [90].

1.06 μm under different temperatures. It is seen that both the transmission and reflection decrease and the absorption coefficient increases with increasing temperature. When the temperature decreases, all the linear optical properties show hysteresis because of the hysteretic twisting of V–V pairs in VO_2. The experimental results show good agreement with the previous literature [74].

Since light is capable of inducing the IMT process, investigating the nonlinear response of VO_2 is difficult for the traditional *Z*-scan technique by using picosecond or femtosecond pulses. Therefore, the VO_2 sample was employed as a saturable modulator to generate pulse lasers, and the kinetic process of the nonlinear response for VO_2 during IMT was analyzed from the pulsed laser performance. The passively *Q*-switched laser at a wavelength of 1.06 μm was demonstrated with a Nd:$GdVO_4$ crystal as the gain medium and the VO_2 sample as the saturable absorber. On the basis of the analysis of Fig. 8(a), it is worth mentioning that the output power during an increasing and a decreasing of the pump power also shows hysteresis. The IMT of VO_2 occurs in the pump range from 2.6 to 5.4 W, corresponding to the temperatures 310 and 360 K, respectively. When the pump power is below 2.6 W, VO_2 is a pure insulator, and the pulse modulation

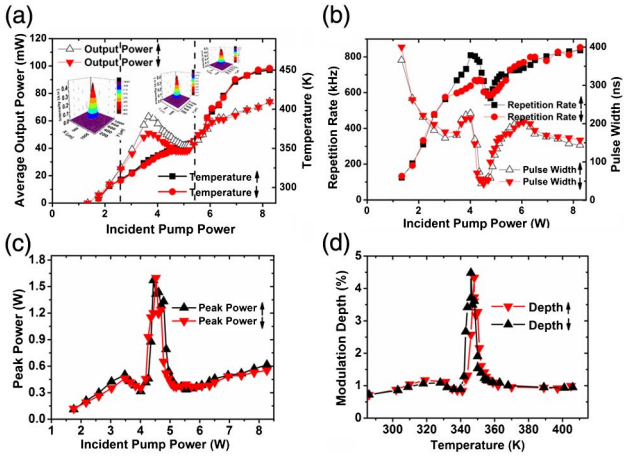

Fig. 8. Laser performance with VO_2 as an optical switch; (a) average output power and central temperature of the laser beam in VO_2 sample recorded during increasing (↑) and decreasing (↓) pump power. Inset: laser patterns achieved with CCD; (b) repetition rate and pulse width during increase (↑) and decrease (↓) of pump power; (c) peak power during increase (↑) and decrease (↓) of pump power; (d) modulation depth with increase (↑) and decrease (↓) of central temperature generated by the pump power. Selected from Ref. [90].

is generated on account of the small band-gap (0.68 eV). When the pump power is above 5.4 W, VO_2 fully becomes a metal material, and the pulse modulation is caused by the saturable properties of the surface plasmon resonance absorption [91–94].

As displayed in Fig. 8(b), it is surprising that a minimum pulse width of 43 ns is obtained at a pump power of 4.4 W, where a break point appeared in the repetition rate, corresponding to a central temperature of 347 K. The result is much better than those of the topological insulator (pulse width of 660 ns) and MoS_2 (pulse width of 970 ns) in the same experimental setup [34,63]. As demonstrated in Fig. 8(d), the modulation depth ΔT could be theoretically calculated by [95]

$$\Delta T = e^{-\alpha_S(\omega)l} - e^{-\alpha(\omega)l} = \frac{3.52T_R}{\tau} \tag{5}$$

where $l = 130$ nm is the thickness of VO_2 thin film, $T_R = 0.54$ ns is the cavity round-trip time, and τ is the pulse width. In addition, as shown in Fig. 9, the variation of saturation intensity and the third-order nonlinear absorption coefficient with changing temperature are elucidated. The largest saturation intensity occurs at 335 K with 21 kW/cm^2, a value much smaller than those of graphene (710 kW/cm^2), Bi_2Se_3 topological insulators (4.3 GW/cm^2), and MoS_2 (2.45 GW/cm^2) [32,34,63]. The lower saturation intensity of VO_2 indicates the sensitive nonlinear optical responses, and the promising application for VO_2 in optoelectronic sensors.

In recent years, VO_2 has received more attention in some areas, including electronics, ultrafast techniques, energy technology, optical storage, and ionic gating [74–76,89–92,96]. By studying the kinetics of the third-order optical nonlinearity during the IMT of VO_2, it is worth noting that VO_2 is of a broad response band (below 1.85 μm) and has fantastic saturable absorption properties in the IMT process. The remarkable *Q*-switched laser with a minimum pulse width of 43 ns and the sensitive nonlinear optical responses all show the utility of phase-transition materials in the development of potential optoelectronic devices.

4. BROADBAND MODULATION BY INHERENT BAND-GAPS

A. Graphene

Graphene is of a very stable honeycomb hexagonal structure assembled by sp^2-hybridized carbon atoms [18,21]. Notwithstanding the significant template for fabricating other

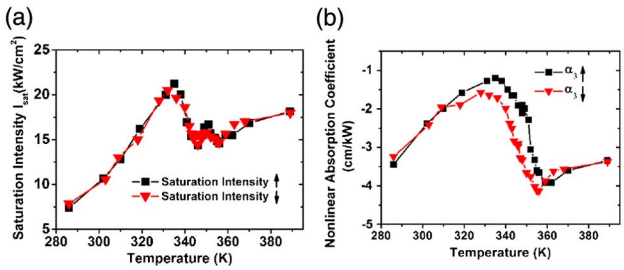

Fig. 9. Nonlinear optical response of VO_2 layer; (a) saturation intensity with increase (↑) and decrease (↓) of central temperature induced by pump power in the IMT process; (b) nonlinear absorption coefficient with increase (↑) and decrease (↓) of central temperature induced by pump power in the IMT process. Selected from Ref. [90].

allotropes of carbon, such as fullerenes, carbon nanotubes, and graphite, graphene was not discovered until 2004 [97], and ironically, the date is later than all these allotropes [22]. For the sp^2 hybridization of graphene, the σ bond is formed by one s orbital and two p orbital (p_x and p_y) electrons between two carbon atoms in the planar structure. The π electron that is the electron in the unaffected p orbital (p_z) is perpendicular to the 2D honeycomb plane. The intercouplings between the electron wave functions of each two nearest π electrons can lead to the formation of a half-filled π band or a half-filled π^* band, corresponding to the valence band and conduction band, respectively [15,22,23].

Zero band-gap of graphene possesses linear dispersion near the Dirac point. Furthermore, this material is insensitive to wavelength, and shows relatively large absorption of visible-to-infrared light (about 2.3% for a monolayer), which all were beneficial for the acquisition of broadband optical response [98–100], As for the carrier dynamics of graphene, the intraband carrier relaxation time and the interband relaxation time are about 10–150 fs and 0.4–1.7 ps, respectively [101–103]. The longer interband relaxation can act as the modulation switching by changing the intrinsic electron and hole carrier densities of graphene. In addition, graphene is also of superior thermal conductivity (5300 W/m/K for a monolayer) [104], large electron mobility of 10^5 $cm^2/V/s$ [18,105], and remarkable elastic properties (a Young's modulus of 1.0 TPa) [106]. As a consequence, graphene is a candidate broadband saturable absorber for the generation of mode-locking or Q-switched pulses.

In 2009, 5 years after the discovery of graphene, the saturable absorption of graphene was first investigated by Q. L. Bao *et al.* [32]. The saturation intensity I_S ranges from 0.61 to 0.71 MW/cm^2 for different layers of graphene, corresponding to the saturation density ranging from 8.16×10^{13} to 5.84×10^{13} [32,107]. This research group also demonstrated the first saturable modulation of graphene in the Er-doped fiber mode-locking laser. The laser oscillation wavelength is about 1.57 μm and the minimum pulse width is about 756 fs. In 2010, the first graphene-based Q-switched laser was presented by Z. Q. Luo *et al.* in the Er-doped fiber with a pulse width of 3.7 μs [108]. Employing a Nd:YAG ceramic medium and a graphene modulator in 2010, W. D. Tan *et al.* reported the first diode-pumped solid-state bulk mode-locking laser with the obtained pulse width of 4 ps at 1.06 μm [64]. Since then, graphene has set off a new wave of research in the mode-locking and Q-switched pulse laser fields. The preparing method causes the prepared graphene saturable absorber to have a low damage threshold and consequently cannot be used in the Q-switching lasers with larger pulse energy than mode-locking lasers.

In the same year of 2010, by means of using graphene epitaxially grown on SiC with high refractive index as the saturable absorber and as the output coupler [109], we obtained the stable passively Q-switched laser for Nd:YAG at 1.06 μm, and it is the first time that the graphene saturable absorber was applied in the Q-switched solid-state pulse laser field. The pulse profiles under different pump power are demonstrated in Fig. 10 and the minimum pulse width is 161 ns. A similar experiment was implemented in the Nd:$LuVO_4$ gain crystal at 1.06 μm, and as shown in Fig. 11, the minimum pulse width is about 56.2 ns [110].

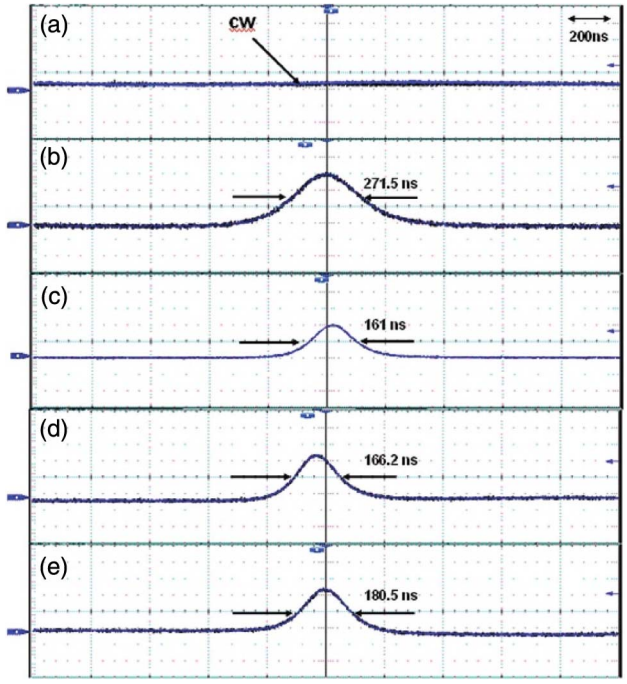

Fig. 10. (a) Display of the cw laser recorded by a digital oscilloscope; (b) Q-switched pulse profile under the pump power of 11.2 W; (c) Q-switched pulse profile under the pump power of 12.9 W; (d) Q-switched pulse profile under the pump power of 14.6 W; (e) Q-switched pulse profile under the pump power of 16.5 W. Selected from Ref. [109].

In addition, recently, graphene was used as a pulse modulator for the generation of a pulsed optical vortex at a wavelength of 1.36 μm in the gain medium of Nd:LYSO [111]. In that experiment, the thermal effect in the Nd:LYSO crystal caused by the large quantum defect of 40.5% is used to do mode-matching selection among different Laguerre–Gaussian ($LG_{p,l}$) modes. As exhibited in Fig. 12, the different $LG_{p,l}$ with corresponding topological charge of $1\hbar$ ($l = 0$, 1, and 2) are directly obtained by controlling the pump power. Corresponding Hermite–Gaussian ($HG_{m,n}$) modes are easily transformed with using two identical cylindrical lenses. Importantly, no topological charge is lost in the whole process suggesting that there is no angular momentum transfer between graphene and vortex pulses such that graphene shows the potential application of generating pulse optical vortices.

B. Bi_2Se_3 Topological Insulator

In recent years, topological insulators (Bi_2Se_3, Bi_2Te_3, and Sb_2Te_3) has drawn great attention in the frontier of science

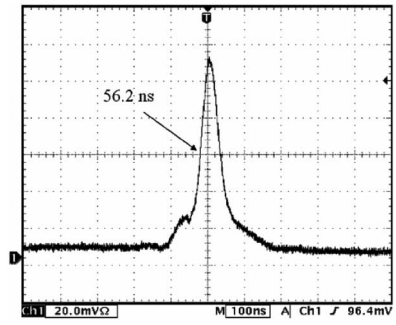

Fig. 11. Pulse profile with the width of 56.2 ns. Selected from Ref. [110].

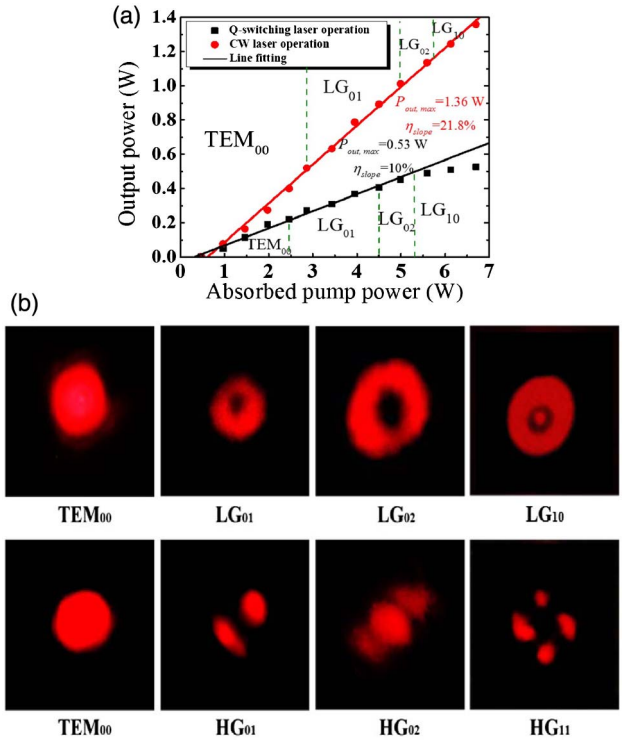

Fig. 12. (a) Continuous wave and pulsed output power of $LG_{p,l}$ modes versus the absorbed pump power; (b) transverse pattern of the laser beam. Top row, achieved $LG_{p,l}$ modes. Bottom row, the converted $HG_{m,n}$ modes corresponding the $LG_{p,l}$ modes. Selected from Ref. [111].

research, due to the exotic physical properties [27,112–118]. Topological insulators show a rhombohedral crystal structure and belong to the space group of $D_{3d}^5(R\bar{3}m)$. Each layer for this kind of materials is of a quintuple-layered sandwich structure along the direction of the 3-fold rotation axis of symmetry; for instance, the layered configuration of Bi_2Se_3 is Se1–Bi1–Se2–Bi1'–Se1'. The coupling between two atomic layers of one quintuple layer is stronger than that between two quintuple layers held together predominantly by the van der Waals forces [113,114].

Two energy states simultaneously exist in topological insulators, and they are the bulk state and the metallic surface state, respectively. Bi_2Se_3 topological insulators have the largest energy gap of the bulk state with a value of about 0.3 eV, and no impurity states exist in the gap [113,115]. The metallic surface state is topological protection with the combination of spin–orbit coupling and time-reversal symmetry against probable scattering [27,116,118]. Similar to graphene, the surface state consists of massless Dirac fermions with a linear energy–momentum relationship. Graphene has two spin-degenerate Dirac cones located at the K and K' points, respectively. Nevertheless, for the Bi_2Se_3 class of topological insulators materials, there is only a single surface Dirac cone around the Γ point with no spin degeneracy [113–115]. Some splendid physical properties were discovered with the gradually in-depth investigations of topological insulators, such as the electromagnetic effect, superconductivity, and quantum anomalous Hall effect [112–115,119,120].

Along with the active research of electronic and magnetic phenomena of topological insulators, its optical characteristic also aroused research interest. Considering the small energy

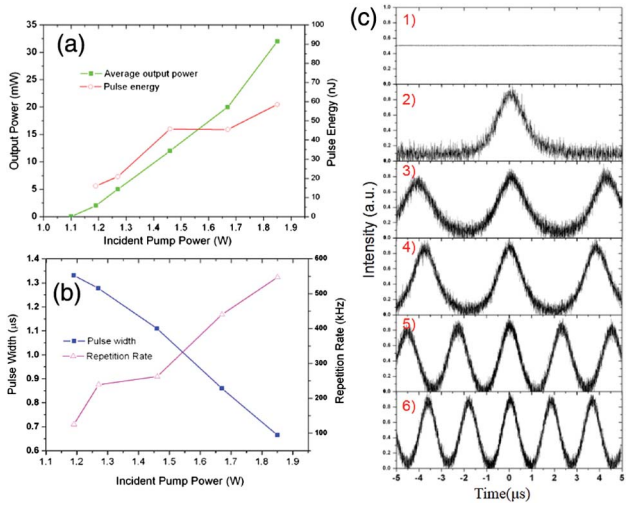

Fig. 13. (a) Average output power and pulse energy vs. increasing incident pump power; (b) pulse width and repetition rate vs. incident pump power; (c) display recorded by digital oscilloscope for lasers. One through 6 are pulse profiles of cw Nd:$GdVO_4$ laser, and pulsed lasers under pump power of 1.19, 1.27, 1.46, 1.67, and 1.85 W, respectively. Selected from Ref. [63].

gap of the bulk state for topological insulators, the saturable absorption was expected to generate under strong excitation with the wavelength not longer than 4.13 μm [114,115]. In 2012, F. Bernard *et al.* discovered that the Bi_2Te_3 topological insulator has saturable absorption at a wavelength of 1.55 μm [121], and then, using the saturable absorber fabricated by Bi_2Te_3 topological insulator and the gain medium of Er-doped fiber, C. J. Zhao *et al.* first obtained the mode-locking lasers with a pulse width of 1.2 ps at 1.56 μm [33].

In 2013, our group demonstrated the stable passively Q-switched laser for Nd:$GdVO_4$ at 1.06 μm with the Bi_2Se_3 topological insulator as the pulse modulator [63]. On the strength of a Z-scan technique, saturable absorption of Bi_2Se_3 saturable modulator was measured and was fitted with Eq. (4). The saturation intensity was determined to be 4.3 GW/cm^2, a value that is much larger than that of graphene (0.61–0.71 MW/cm^2) [32,63]. The output power and pulse profiles under different pump power are demonstrated in Fig. 13, and the minimum pulse width is about 666 ns. Employing the same Bi_2Se_3 saturable absorber, a dual-wavelength simultaneously Q-switched Nd:Lu_2O_3 laser was also achieved [122]. As shown in Fig. 14, the shortest pulse width is about 720 ns and the laser wavelengths are 1077 and 1081 nm, respectively.

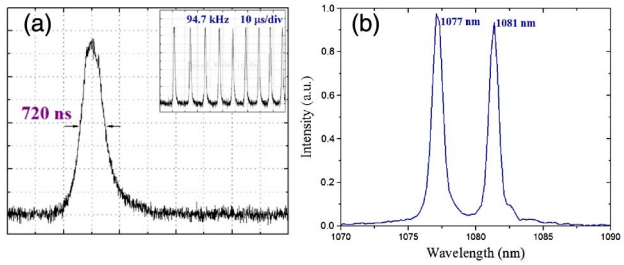

Fig. 14. (a) Single-pulse profile with duration of 720 ns. Inset, corresponding pulse train with the repetition rate of 94.7 kHz; (b) laser spectrum of the dual-wavelength laser at 1077 and 1081 nm. Selected from Ref. [122].

At the beginning of pulse modulation for topological insulators (Bi_2Se_3, Bi_2Te_3, and Sb_2Te_3), the *Q*-switched or mode-locking lasers are concentrated on the wavelengths from 1 to 1.6 μm in the gain media such as Nd:$GdVO_4$ [63], Yb-doped fibers [123], Er-doped fibers [33,124–126], and Er:YAG ceramic [127]. In 2014, M. W. Jung reported the mode-locked femtosecond pulse laser at 1935 nm with Bi_2Te_3 topological insulator as the saturable absorber and the Tm/Ho co-doped fiber as the gain medium [128]. Soon after, Z. Q. Luo *et al.* demonstrated a *Q*-switched double-clad single-mode Tm^{3+}-doped fiber laser at 2 μm wavelength with Bi_2Se_3 topological insulator as the saturable modulator [129]. These two experiments confirm the broadband saturable modulation of topological insulators with the applicable wavelength expanded to 2 μm or longer wavelengths.

5. CONCLUSIONS

In this paper, on the basis of the band-gap modulation, some latest research results about 2D broadband saturable absorbers, including MoS_2 and VO_2, graphene, and Bi_2Se_3 topological insulator were systematically elucidated and reviewed. For the few-layer MoS_2, the broadband pulse modulation was achieved from 1.06 to 2.1 μm by introducing appropriate S defects to reduce the intrinsic band-gap. For the VO_2 IMT, the transition process from the insulator phase to metal phase resulted in some fantastic results in terms of pulse modulation, such as small pulse widths and sensitive nonlinear optical responses. In addition, with respect to graphene and Bi_2Se_3 topological insulator, the small inherent bandgaps leaded to the success of broadband saturated absorption. As a consequence, this work shows the excellent performance of band-gap engineering for exploring 2D broadband saturable materials, and importantly, it opens up an available application opportunity for 2D materials in photonics and optoelectronics.

ACKNOWLEDGMENTS

This work was supported by the National Natural Science Foundation of China (Nos. 51025210 and 51422205) and the China Scholarship Council in 2014 (No. 201406220045).

REFERENCES

1. T. H. Maiman, "Stimulated optical radiation in ruby," Nature **187**, 493–494 (1960).
2. U. Keller, "Recent developments in compact ultrafast lasers," Nature **424**, 831–838 (2003).
3. H. Yu, J. Liu, H. Zhang, A. A. Kaminskii, Z. Wang, and J. Wang, "Advances in vanadate laser crystals at a lasing wavelength of 1 micrometer," Laser Photon. Rev. **8**, 847–864 (2014).
4. F. Bonaccorso, Z. Sun, T. Hasan, and A. C. Ferrari, "Graphene photonics and optoelectronics," Nat. Photonics **4**, 611–622 (2010).
5. Y. Shimony, Z. Burshtein, and Y. Kalisky, "Cr^{4+}:YAG as passive Q-switch and Brewster plate in a pulsed Nd:YAG laser," IEEE J. Quantum Electron. **31**, 1738–1741 (1995).
6. T. Y. Tsai and M. Birnbaum, "Q-switched 2-μm lasers by use of a Cr^{2+}:ZnSe saturable absorber," Appl. Opt. **40**, 6633–6637 (2001).
7. A. M. Malyarevich, I. A. Denisov, K. V. Yumashev, V. P. Mikhailov, R. S. Conroy, and B. D. Sinclair, "V:YAG–A new passive Q-switch for diode-pumped solid-state lasers," Appl. Phys. B **67**, 555–558 (1998).
8. U. Keller, D. A. B. Miller, G. D. Boyd, T. H. Chiu, J. F. Ferguson, and M. T. Asom, "Solid-state low-loss intracavity saturable absorber for Nd:YLF lasers: An antiresonant semiconductor Fabry–Perot saturable absorber," Opt. Lett. **17**, 505–507 (1992).
9. T. T. Basiev, S. B. Mirov, and V. V. Osiko, "Room-temperature color center lasers," IEEE J. Quantum Electron. **24**, 1052–1069 (1988).
10. U. Keller and A. C. Tropper, "Passively modelocked surface-emitting semiconductor lasers," Phys. Rep. **429**, 67–120 (2006).
11. X. P. Hu, P. Xu, and S. N. Zhu, "Engineered quasi-phase-matching for laser techniques [Invited]," Photon. Res. **1**, 171–185 (2013).
12. Y. F. Chen, S. W. Tsai, and S. C. Wang, "High-power diode-pumped nonlinear mirror mode-locked Nd:YVO_4 laser with periodically-poled KTP," Appl. Phys. B **72**, 395–397 (2001).
13. Y. H. Liu, Z. D. Xie, S. D. Pan, X. J. Lv, Y. Yuan, X. P. Hu, J. Lu, L. N. Zhao, C. D. Chen, G. Zhao, and S. N. Zhu, "Diode-pumped passively mode-locked Nd:YVO_4 laser at 1342 nm with periodically poled $LiTaO_3$," Opt. Lett. **36**, 698–700 (2011).
14. K. S. Novoselov, V. I. Fal, L. Colombo, P. R. Gellert, M. G. Schwab, and K. Kim, "A roadmap for graphene," Nature **490**, 192–200 (2012).
15. C. N. R. Rao, A. K. Sood, K. S. Subrahmanyam, and A. Govindaraj, "Graphene: The new two-dimensional nanomaterial," Angew. Chem.. Int. Ed. Engl., Suppl. **48**, 7752–7777 (2009).
16. S. Z. Butler, S. M. Hollen, L. Cao, Y. Cui, J. A. Gupta, H. R. Gutiérrez, T. F. Heinz, S. S. Hong, J. Huang, A. F. Ismach, E. Johnston-Halperin, M. Kuno, V. V. Plashnitsa, R. D. Robinson, R. S. Ruoff, S. Salahuddin, J. Shan, L. Shi, M. G. Spencer, M. Terrones, W. Windl, and J. E. Goldberger, "Progress, challenges, and opportunities in two-dimensional materials beyond graphene," ACS Nano **7**, 2898–2926 (2013).
17. M. Xu, T. Liang, M. Shi, and H. Chen, "Graphene-like two-dimensional materials," Chem. Rev. **113**, 3766–3798 (2013).
18. A. K. Geim and K. S. Novoselov, "The rise of graphene," Nat. Mater. **6**, 183–191 (2007).
19. K. S. Novoselov, D. Jiang, F. Schedin, T. J. Booth, V. V. Khotkevich, S. V. Morozov, and A. K. Geim, "Two-dimensional atomic crystals," Proc. Natl. Acad. Sci. USA **102**, 10451–10453 (2005).
20. K. S. Novoselov, A. K. Geim, S. V. Morozov, D. Jiang, M. I. Katsnelson, I. V. Grigorieva, S. V. Dubonos, and A. A. Firsov, "Two-dimensional gas of massless Dirac fermions in graphene," Nature **438**, 197–200 (2005).
21. K. P. Loh, Q. Bao, P. K. Ang, and J. Yang, "The chemistry of graphene," J. Mater. Chem. **20**, 2277–2289 (2010).
22. A. H. C. Neto, F. Guinea, N. M. R. Peres, K. S. Novoselov, and A. K. Geim, "The electronic properties of graphene," Rev. Mod. Phys. **81**, 109–162 (2009).
23. P. R. Wallace, "The band theory of graphite," Phys. Rev. **71**, 622–634 (1947).
24. A. K. Geim and I. V. Grigorieva, "Van der Waals heterostructures," Nature **499**, 419–425 (2013).
25. Q. H. Wang, K. Kalantar-Zadeh, A. Kis, J. N. Coleman, and M. S. Strano, "Electronics and optoelectronics of two-dimensional transition metal dichalcogenides," Nat. Nanotechnol. **7**, 699–712 (2012).
26. Z. He, C. Zhong, S. Su, M. Xu, H. Wu, and Y. Cao, "Enhanced power-conversion efficiency in polymer solar cells using an inverted device structure," Nat. Photonics **6**, 591–595 (2012).
27. Y. Zhang, K. He, C. Z. Chang, C. L. Song, L. L. Wang, X. Chen, J. F. Jia, Z. Fang, X. Dai, W. Y. Shan, S. Q. Shen, Q. Niu, X. L. Qi, S. C. Zhang, X. C. Ma, and Q. K. Xue, "Crossover of the three-dimensional topological insulator Bi_2Se_3 to the two-dimensional limit," Nat. Phys. **6**, 584–588 (2010).
28. C. C. Liu, W. Feng, and Y. Yao, "Quantum spin Hall effect in silicene and two-dimensional germanium," Phys. Rev. Lett. **107**, 076802 (2011).
29. L. Li, Y. Yu, G. J. Ye, Q. Ge, X. Ou, H. Wu, D. Feng, X. H. Chen, and Y. Zhang, "Black phosphorus field-effect transistors," Nat. Nanotechnol. **9**, 372–377 (2014).
30. J. Qiao, X. Kong, Z. X. Hu, F. Yang, and W. Ji, "High-mobility transport anisotropy and linear dichroism in few-layer black phosphorus," Nat. Commun. **5**, 4475 (2014).
31. J. N. Coleman, M. Lotya, A. O'Neill, S. D. Bergin, P. J. King, U. Khan, K. Young, A. Gaucher, S. De, R. J. Smith, I. V. Schvets, S. K. Arora, G. Stanton, H. Kim, K. Lee, G. T. Kim, G. S. Duesberg, T. Hallam, J. J. Boland, J. J. Wang, J. F. Donegan, J. C. Grunlan, G. Moriarty, A. Shmeliov, R. J. Nicholls, J. M. Perkins, E. M. Grieveson, K. Theuwissen, D. W. McComb, P. D. Nellist, and

V. Nicolosi, "Two-dimensional nanosheets produced by liquid exfoliation of layered materials," Science **331**, 568–571 (2011).
32. Q. Bao, H. Zhang, Y. Wang, Z. Ni, Y. Yan, Z. Shen, K. Loh, and D. Tang, "Atomic-layer graphene as a saturable absorber for ultrafast pulsed lasers," Adv. Funct. Mater. **19**, 3077–3083 (2009).
33. C. Zhao, H. Zhang, X. Qi, Y. Chen, Z. Wang, S. Wen, and D. Tang, "Ultra-short pulse generation by a topological insulator based saturable absorber," Appl. Phys. Lett. **101**, 211106 (2012).
34. S. Wang, H. Yu, H. Zhang, A. Wang, M. Zhao, Y. Che, L. Mei, and J. Wang, "Broadband few-layer MoS_2 saturable absorbers," Adv. Mater. **26**, 3538–3544 (2014).
35. L. Ci, L. Song, C. Jin, D. Jariwala, D. Wu, Y. Li, A. Srivastava, Z. F. Wang, K. Storr, L. Balicas, F. Liu, and P. M. Ajayan, "Atomic layers of hybridized boron nitride and graphene domains," Nat. Mater. **9**, 430–435 (2010).
36. S. Helveg, J. V. Lauritsen, E. Lægsgaard, I. Stensgaard, J. K. Nørskov, B. S. Clausen, H. Topsøe, and F. Besenbacher, "Atomic-scale structure of single-layer MoS_2 nanoclusters," Phys. Rev. Lett. **84**, 951–954 (2000).
37. S. Wu, J. S. Ross, G. B. Liu, G. Aivazian, A. Jones, Z. Fei, W. Zhu, D. Xiao, W. Yao, D. Cobden, and X. Xu, "Electrical tuning of valley magnetic moment through symmetry control in bilayer MoS_2," Nat. Phys. **9**, 149–153 (2013).
38. B. Radisavljevic, A. Radenovic, J. Brivio, V. Giacometti, and A. Kis, "Single-layer MoS_2 transistors," Nat. Nanotechnol. **6**, 147–150 (2011).
39. R. A. Gordon, D. Yang, E. D. Crozier, D. T. Jiang, and R. F. Frindt, "Structures of exfoliated single layers of WS_2, MoS_2, and $MoSe_2$ in aqueous suspension," Phys. Rev. B **65**, 125407 (2002).
40. H. S. S. Ramakrishna Matte, A. Gomathi, A. K. Manna, D. J. Late, R. Datta, S. K. Pati, and C. N. R. Ra, "MoS_2 and WS_2 analogues of graphene," Angew. Chem. **122**, 4153–4156 (2010).
41. T. Li and G. Galli, "Electronic properties of MoS_2 nanoparticles," J. Phys. Chem. C **111**, 16192–16196 (2007).
42. K. K. Kam and B. A. Parkinson, "Detailed photocurrent spectroscopy of the semiconducting group VIB transition metal dichalcogenides," J. Phys. Chem. **86**, 463–467 (1982).
43. A. Splendiani, L. Sun, Y. Zhang, T. Li, J. Kim, C. Y. Chim, G. Galli, and F. Wang, "Emerging photoluminescence in monolayer MoS_2," Nano Lett. **10**, 1271–1275 (2010).
44. R. Coehoorn, C. Haas, J. Dijkstra, C. J. F. Flipse, R. A. D. Groot, and A. Wold, "Electronic structure of $MoSe_2$, MoS_2, and WSe_2. I. Band-structure calculations and photoelectron spectroscopy," Phys. Rev. B **35**, 6195–6202 (1987).
45. J. S. Qi, X. Li, X. F. Qian, and J. Feng, "Bandgap engineering of rippled MoS_2 monolayer under external electric field," Appl. Phys. Lett. **102**, 173112 (2013).
46. H. J. Conley, B. Wang, J. I. Ziegler, R. F. Haglund, Jr., S. T. Pantelides, and K. I. Bolotin, "Bandgap engineering of strained monolayer and bilayer MoS_2," Nano Lett. **13**, 3626–3630 (2013).
47. A. Castellanos-Gomez, R. Roldán, E. Cappelluti, M. Buscema, F. Guinea, H. S. J. van der Zant, and G. A. Steele, "Local strain engineering in atomically thin MoS_2," Nano Lett. **13**, 5361–5366 (2013).
48. Q. H. Liu, L. Z. Y. F. Li, Z. X. Gao, Z. F. Chen, and J. Lu, "Tuning electronic structure of bilayer MoS_2 by vertical electric field: A first-principles investigation," J. Phys. Chem. C **116**, 21556–21562 (2012).
49. Y. Kim, J. L. Huang, and C. M. Lieber, "Characterization of nanometer scale wear and oxidation of transition metal dichalcogenide lubricants by atomic force microscopy," Appl. Phys. Lett. **59**, 3404–3406 (1991).
50. A. Carvalho, R. M. Ribeiro, and A. H. C. Neto, "Band nesting and the optical response of two-dimensional semiconducting transition metal dichalcogenides," Phys. Rev. B **88**, 115205 (2013).
51. L. Britnell, R. M. Ribeiro, A. Eckmann, R. Jalil, B. D. Belle, A. Mishchenko, Y.-J. Kim, R. V. Gorbachev, T. Georgiou, S. V. Morozov, A. N. Grigorenko, A. K. Geim, C. Casiraghi, A. H. C. Neto, and K. S. Novoselov, "Strong light-matter interactions in heterostructures of atomically thin films," Science **340**, 1311–1314 (2013).
52. R. Wang, B. A. Ruzicka, N. Kumar, M. Z. Bellus, H. Y. Chiu, and H. Zhao, "Ultrafast and spatially resolved studies of charge carriers in atomically thin molybdenum disulfide," Phys. Rev. B **86**, 045406 (2012).
53. N. Kumar, S. Najmaei, Q. Cui, F. Ceballos, P. M. Ajayan, J. Lou, and H. Zhang, "Second harmonic microscopy of monolayer MoS_2," Phys. Rev. B **87**, 161403 (2013).
54. J. Strait, P. Nene, H. Wang, C. Zhang, and F. Rana, "Carrier relaxation dynamics in MoS_2 measured by optical/THz pump-probe spectroscopy," in *Conference on Lasers and Electro-Optics (CLEO)*, Technical Digest Series (OSA, 2013), paper JTh2A.37.
55. H. Wang, C. Zhang, and F. Rana, "Ultrafast carrier dynamics in single and few layer MoS_2 studied by optical pump probe technique," in *Conference on Lasers and Electro-Optics (CLEO)*, Technical Digest Series (OSA, 2013), paper QTu1D.2.
56. K. Wang, J. Wang, J. Fan, M. Lotya, A. O'Neill, D. Fox, Y. Feng, X. Zhang, B. Jiang, Q. Zhao, H. Zhang, J. N. Coleman, L. Zhang, and W. J. Blau, "Ultrafast saturable absorption of two-dimensional MoS_2 nanosheets," ACS Nano **7**, 9260–9267 (2013).
57. O. Madelung, *Introduction to Solid-State Theory*, Vol. **2** (Springer, 1996), Chap. 8 and 9.
58. G. Kresse and J. Furthmuller, "Efficiency of ab-initio total energy calculations for metals and semiconductors using a plane-wave basis set," Comput. Mater. Sci. **6**, 15–50 (1996).
59. G. Kresse and J. Furthmüller, "Efficient iterative schemes for ab initio total-energy calculations using a plane-wave basis set," Phys. Rev. B **54**, 11169–11186 (1996).
60. V. Yu. Fominski, V. N. Nevolin, R. I. Romanov, and I. Smurov, "Ion-assisted deposition of MoSx films from laser-generated plume under pulsed electric field," J. Appl. Phys. **89**, 1449–1457 (2001).
61. E. Garmire and A. Kost, "Resonant optical nonlinearities in semiconductors," in *Nonlinear Optics in Semiconductor I*, R. K. Willardson and E. R. Weber, eds. (Academic, 1999), pp. 2–50.
62. E. Garmire, "Resonant optical nonlinearities in semiconductors," IEEE J. Sel. Top. Quantum Electron. **6**, 1094–1110 (2000).
63. H. Yu, H. Zhang, Y. Wang, C. Zhao, B. Wang, S. Wen, H. Zhang, and J. Wang, "Topological insulator as an optical modulator for pulsed solid-state lasers," Laser Photon. Rev. **7**, L77–L83 (2013).
64. W. D. Tan, C. Y. Su, R. J. Knize, G. Q. Xie, L. J. Li, and D. Tang, "Mode locking of ceramic Nd:yttrium aluminum garnet with graphene as a saturable absorber," Appl. Phys. Lett. **96**, 031106 (2010).
65. J. Du, Q. Wang, G. Jiang, C. Xu, C. Zhao, Y. Xiang, Y. Chen, S. Wen, and H. Zhang, "Ytterbium-doped fiber laser passively mode locked by few-layer molybdenum disulfide (MoS_2) saturable absorber functioned with evanescent field interaction," Sci. Rep. **4**, 6346 (2014).
66. H. Zhang, S. B. Lu, J. Zheng, J. Du, S. C. Wen, D. Y. Tang, and K. P. Loh, "Molybdenum disulfide (MoS_2) as a broadband saturable absorber for ultra-fast photonics," Opt. Express **22**, 7249–7260 (2014).
67. H. Liu, A. Luo, F. Wang, R. Tang, M. Liu, Z. Luo, W. Xu, C. Zhao, and H. Zhang, "Femtosecond pulse erbium-doped fiber laser by a few-layer MoS_2 saturable absorber," Opt. Lett. **39**, 4591–4594 (2014).
68. M. Liu, X. W. Zheng, Y. L. Qi, H. Liu, A. Luo, Z. C. Luo, W. C. Xu, C. J. Zhao, and H. Zhang, "Microfiber-based few-layer MoS_2 saturable absorber for 2.5 GHz passively harmonic mode-locked fiber laser," Opt. Express **22**, 22841–22846 (2014).
69. R. Khazaeizhad, S. H. Kassani, H. Jeong, D. I. Yeom, and K. Oh, "Mode-locking of Er-doped fiber laser using a multilayer MoS_2 thin film as a saturable absorber in both anomalous and normal dispersion regimes," Opt. Express **22**, 23732–23742 (2014).
70. Y. Z. Huang, Z. Q. Y. Y. Luo, Y. Y. Li, M. Zhong, B. Xu, K. J. Che, H. Y. Xu, Z. P. Cai, J. Peng, and J. Weng, "Widely-tunable, passively Q-switched erbium-doped fiber laser with few-layer MoS_2 saturable absorber," Opt. Express **22**, 25258–25266 (2014).
71. Z. Luo, Y. Huang, M. Zhong, Y. Li, J. Wu, B. Xu, H. Xu, Z. Cai, J. Peng, and J. Weng, "1, 1.5 and 2 μm fiber lasers Q-switched by a broadband few-layer MoS_2 saturable absorber," J. Lightwave Technol. **32**, 4077–4084 (2014).
72. J. Bardeen, L. N. Cooper, and J. R. Schrieffer, "Theory of superconductivity," Phys. Rev. **108**, 1175–1204 (1957).

73. C. Haas, "Phase transitions in ferroelectric and antiferroelectric crystals," Phys. Rev. **140**, A863–A868 (1965).
74. M. M. Qazilbash, M. Brehm, B.-G. Chae, P.-C. Ho, G. O. Andreev, B.-J. Kim, S. J. Yun, A. V. Balatsky, M. B. Maple, F. Keilmann, H.-T. Kim, and D. N. Basov, "Mott transition in VO_2 revealed by infrared spectroscopy and nano-imaging," Science **318**, 1750–1753 (2007).
75. N. B. Aetukuri, A. X. Gray, M. Drouard, M. Cossale, L. Gao, A. H. Reid, R. Kukreja, H. Ohldag, C. A. Jenkins, E. Arenholz, K. P. Roche, H. A. Dürr, M. G. Samant, and S. S. P. Parkin, "Control of the metal-insulator transition in vanadium dioxide by modifying orbital occupancy," Nat. Phys. **9**, 661–666 (2013).
76. M. Nakano, K. Shibuya, D. Okuyama, T. Hatano, S. Ono, M. Kawasaki, Y. Iwasa, and Y. Tokura, "Collective bulk carrier delocalization driven by electrostatic surface charge accumulation," Nature **487**, 459–462 (2012).
77. M. Liu, H. Y. Hwang, H. Tao, A. Strikwerda, K. Fan, G. R. Keiser, A. J. Sternbach, K. G. West, S. Kittiwatanakul, J. Lu, S. A. Wolf, F. G. Omenetto, X. Zhang, K. A. Nelson, and R. D. Averitt, "Terahertz-field-induced insulator-to-metal transition in vanadium dioxide metamaterial," Nature **487**, 345–348 (2012).
78. V. Eyert, "VO2: A novel view from band theory," Phys. Rev. Lett. **107**, 016401 (2011).
79. M. Imada, A. Fujimori, and Y. Tokura, "Metal–insulator transitions," Rev. Mod. Phys. **70**, 1039–1263 (1998).
80. T. Yao, X. Zhang, Z. Sun, S. Liu, Y. Huang, Y. Xie, C. Wu, X. Yuan, W. Zhang, Z. Wu, G. Pan, F. Hu, L. Wu, Q. Liu, and S. Wei, "Understanding the nature of the kinetic process in a VO_2 metal–insulator transition," Phys. Rev. Lett. **105**, 226405 (2010).
81. J. Jeong, N. Aetukuri, T. Graf, T. D. Schladt, M. G. Samant, and S. S. P. Parkin, "Suppression of metal–insulator transition in VO_2 by electric field-induced oxygen vacancy formation," Science **339**, 1402–1405 (2013).
82. J. B. Goodenough, "Direct cation–cation interactions in several oxides," Phys. Rev. **117**, 1442–1451 (1960).
83. T. C. Koethe, Z. Hu, M. W. Haverkort, C. Schüßler-Langeheine, F. Venturini, N. B. Brookes, O. Tjernberg, W. Reichelt, H. H. Hsieh, H.-J. Lin, C. T. Chen, and L. H. Tjeng, "Transfer of spectral weight and symmetry across the metal-insulator transition in VO_2," Phys. Rev. Lett. **97**, 116402 (2006).
84. S. Biermann, A. Poteryaev, A. I. Lichtenstein, and A. Georges, "Dynamical singlets and correlation-assisted Peierls transition in VO_2," Phys. Rev. Lett. **94**, 026404 (2005).
85. A. Cavalleri, T. Dekorsy, H. H. W. Chong, J. C. Kiedder, and R. W. Schoenlein, "Evidence for a structurally-driven insulator-to-metal transition in VO_2: A view from the ultrafast timescale," Phys. Rev. B **70**, 161102 (2004).
86. P. Limelette, A. Georges, D. Jérome, P. Wzietek, P. Metaclf, and J. M. Honig, "Universality and critical behavior at the Mott transition," Science **302**, 89–92 (2003).
87. A. Cavalleri, C. Tóth, C. W. Siders, J. A. Squier, and F. Ráksi, "Femtosecond structural dynamics in VO_2 during an ultrafast solid-solid phase transition," Phys. Rev. Lett. **87**, 237401 (2001).
88. J. Umeda, H. Kusumoto, K. Narita, and E. Yamada, "Nuclear magnetic resonance in polycrystalline VO_2," J. Chem. Phys. **42**, 1458–1459 (1965).
89. J. H. Park, J. M. Coy, T. S. Kasirga, C. Huang, Z. Fei, S. Hunter, and D. H. Gobden, "Measurement of a solid-state triple point at the metal-insulator transition in VO_2," Nature **500**, 431–434 (2013).
90. H. Yu, S. Wang, A. Wang, M. Zhao, H. Zhang, Y. Chen, L. Mei, and J. Wang, "Kinetics of nonlinear optical response at insulator-metal transition in vanadium dioxide," Adv. Opt. Mater. **3**, 64–70 (2015)
91. L. Wang, E. Radue, S. Kittiwatanakul, C. Clavero, J. Lu, S. A. Wolf, I. Novikova, and R. A. Lukaszew, "Surface plasmon polaritons in VO_2 thin films for tunable low-loss plasmonic applications," Opt. Lett. **37**, 4335–4337 (2012).
92. M. Rini, A. Cavalleri, R. W. Schoenlein, R. López, L. C. Feldman, R. F. Haglund, L. A. Boatner, and T. E. Haynes, "Photoinduced phase transition in VO_2 nanocrystals: Ultrafast control of surface-plasmon resonance," Opt. Lett. **30**, 558–560 (2005).
93. B. A. Kruger, A. Joushaghani, and J. K. S. Poon, "Design of electrically driven hybrid vanadium dioxide (VO_2) plasmonic switches," Opt. Express **20**, 23598–23609 (2012).
94. Y. Zhou, A. Huang, Y. Li, S. Ji, Y. Gao, and P. Jin, "Surface plasmon resonance induced excellent solar control for VO_2@SiO_2 nanorods-based thermochromic foils," Nanoscale **5**, 9208–9213 (2013).
95. X. Zhang, S. Zhao, Q. Wang, Q. Zhang, L. Sun, and S. Zhang, "Optimization of Cr4+-doped saturable-absorber Q-switched lasers," IEEE J. Quantum Electron. **33**, 2286–2294 (1997).
96. C. Kübler, H. Ehrke, R. Huber, R. Lopez, A. Halabica, R. F. Haglund, Jr., and A. Leitenstorfer, "Coherent structural dynamics and electronic correlations during an ultrafast insulator-to-metal phase transition in VO_2," Phys. Rev. Lett. **99**, 116401 (2007).
97. K. S. Novoselov, A. K. Geim, S. V. Morozov, D. Jiang, Y. Zhang, S. V. Dubonos, I. V. Grigorieva, and A. A. Firsov, "Electric field effect in atomically thin carbon films," Science **306**, 666–669 (2004).
98. A. B. Kuzmenko, E. V. Heumen, F. Carbone, and D. V. D. Marel, "Universal optical conductance of graphite," Phys. Rev. Lett. **100**, 117401 (2008).
99. R. R. Nair, P. Blake, A. N. Grigorenko, K. S. Novoselov, T. J. Booth, T. Stauber, N. M. R. Peres, and A. K. Geim, "Fine structure constant defines visual transparency of graphene," Science **320**, 1308 (2008).
100. Z. Q. Li, E. A. Henriksen, Z. Jiang, Z. Hao, M. C. Martin, P. Kim, H. L. Stormer, and D. N. Basov, "Dirac charge dynamics in graphene by infrared spectroscopy," Nat. Phys. **4**, 532–535 (2008).
101. J. M. Dawlaty, S. Shivaraman, M. Chandrashekhar, F. Rana, and M. G. Spencer, "Measurement of ultrafast carrier dynamics in epitaxial graphene," Appl. Phys. Lett. **92**, 042116 (2008).
102. P. A. George, J. Strait, J. Dawlaty, S. Shivaraman, M. Chandrashekhar, F. Rana, and M. G. Spencer, "Ultrafast optical-pump terahertz-probe spectroscopy of the carrier relaxation and recombination dynamics in epitaxial graphene," Nano Lett. **8**, 4248–4251 (2008).
103. M. Breusing, C. Ropers, and T. Elsaesser, "Ultrafast carrier dynamics in graphite," Phys. Rev. Lett. **102**, 086809 (2009).
104. A. A. Balandin, S. Ghosh, W. Bao, I. Calizo, D. teweldebrhan, F. Miao, and C. N. Lau, "Superior thermal conductivity of single-layer graphene," Nano Lett. **8**, 902–907 (2008).
105. S. V. Morozov, K. S. Novoselov, M. I. Katsnelson, F. Schedin, D. C. Elias, J. A. Jaszczak, and A. K. Geim, "Giant intrinsic carrier mobilities in graphene and its bilayer," Phys. Rev. Lett. **100**, 016602 (2008).
106. C. Lee, X. Wei, J. W. Kysar, and J. Hone, "Measurement of the elastic properties and intrinsic strength of monolayer graphene," Science **321**, 385–388 (2008).
107. H. Zhang, S. Virally, Q. Bao, K. P. Loh, S. Massar, N. Godbout, and P. Kockaert, "Z-scan measurement of the nonlinear refractive index of graphene," Opt. Lett. **37**, 1856–1858 (2012).
108. Z. Luo, M. Zhou, J. Weng, G. M. Huang, H. Y. Xu, C. C. Ye, and Z. P. Cai, "Graphene-based passively Q-switched dual-wavelength erbium-doped fiber laser," Opt. Lett. **35**, 3709–3711 (2010).
109. H. Yu, X. Chen, H. Zhang, X. Xu, X. Hu, Z. Wang, J. Wang, S. Zhuang, and M. Jiang, "Large energy pulse generation modulated by graphene epitaxially grown on silicon carbide," ACS Nano **4**, 7582–7586 (2010).
110. H. Yu, X. Chen, X. Hu, S. Zhuang, Z. Wang, X. Xu, J. Wang, H. Zhang, and M. Jiang, "Graphene as a Q-switcher for neodymium-doped lutetium vanadate laser," Appl. Phys. Express **4**, 022704 (2011).
111. Y. Ding, M. Xu, Y. Zhao, H. Yu, H. Zhang, Z. Wang, and J. Wang, "Thermally driven continuous-wave and pulsed optical vortex," Opt. Lett. **39**, 2366–2369 (2014).
112. C. Z. Chang, J. Zhang, X. Feng, J. Shen, Z. Zhang, M. Guo, K. Li, Y. Ou, P. Wei, L. L. Wang, Z. Q. Ji, Y. Feng, S. Ji, X. Chen, J. Jia, X. Dai, Z. Fang, S. C. Zhang, K. He, Y. Wang, L. Lu, X. C. Ma, and Q. K. Xue, "Experimental observation of the quantum anomalous Hall effect in a magnetic topological insulator," Science **340**, 167–170 (2013).
113. Y. L. Chen, J. G. Analytis, J. H. Chu, Z. K. Liu, S. K. Mo, X. L. Qi, H. J. Zhang, D. H. Lu, X. Dai, Z. Fang, S. C. Zhang, I. R. Fisher, Z. Hussain, and Z. X. Shen, "Experimental realization of a three-dimensional topological insulator, Bi_2Te_3," Science **325**, 178–181 (2009).

114. H. Zhang, C. X. Liu, X. L. Qi, X. Dai, Z. Fang, and S. C. Zhang, "Topological insulators in Bi_2Se_3, Bi_2Te_3 and Sb_2Te_3 with a single Dirac cone on the surface," Nat. Phys. **5**, 438–442 (2009).
115. Y. Xia, D. Qian, D. Hsieh, L. Wray, A. Pal, H. Lin, A. Bansil, D. Grauer, Y. S. Hor, R. J. Cava, and M. Z. Hasan, "Observation of a large-gap topological-insulator class with a single Dirac cone on the surface," Nat. Phys. **5**, 398–402 (2009).
116. J. E. Moore, "The birth of topological insulators," Nature **464**, 194–198 (2010).
117. J. G. Analytis, R. D. McDonald, S. C. Riggs, J. H. Chu, G. S. Boebinger, and L. R. Fisher, "Two-dimensional surface state in the quantum limit of a topological insulator," Nat. Phys. **6**, 960–964 (2010).
118. J. Moore, "Topological insulators: The next generation," Nat. Phys. **5**, 378–380 (2009).
119. M. Veldhorst, M. Snelder, M. Hoek, T. Gang, V. K. Guduru, X. L. Wang, U. Zeitler, W. G. van der Wiel, A. A. Golubov, H. Hilgenkamp, and A. Brinkman, "Josephson supercurrent through a topological insulator surface state," Nat. Mater. **11**, 417–421 (2012).
120. Y. L. Chen, J. H. Chu, J. G. Analytis, Z. K. Liu, K. Lgarashi, H. H. Kuo, S. K. Mo, R. G. Moore, D. H. Lu, M. Hashimoto, T. Sasagawa, S. C. Zhang, I. R. Fisher, Z. Hussain, and Z. X. Shen, "Massive Dirac fermion on the surface of a magnetically doped topological insulator," Science **329**, 659–662 (2010).
121. F. Bernard, H. Zhang, S. P. Gorza, and P. Emplit, "Towards mode-locked fiber laser using topological insulators," in *Nonlinear Photonics*, OSA Digest Series (OSA, 2012) paper NTh1A.5.
122. B. Wang, H. Yu, H. Zhang, C. Zhao, S. Wen, H. Zhang, and J. Wang, "Topological insulator simultaneously Q-switched dual-wavelength Nd:Lu_2O_3 laser," IEEE J. Photon. **6**, 1501007 (2014).
123. Z. Luo, Y. Huang, J. Weng, H. Cheng, Z. Lin, B. Xu, Z. Cai, and H. Xu, "1.06 μm Q-switched ytterbium-doped fiber laser using few-layer topological insulator Bi_2Se_3 as a saturable absorber," Opt. Express **21**, 29516–29522 (2013).
124. C. Zhao, Y. Zou, Y. Chen, Z. Wang, S. Lu, H. Zhang, S. Wen, and D. Tang, "Wavelength-tunable picosecond soliton fiber laser with topological insulator: Bi_2Se_3 as a mode locker," Opt. Express **20**, 27888–27895 (2012).
125. Y. Chen, C. Zhao, H. Huang, S. Chen, P. Tang, Z. Wang, S. Lu, H. Zhang, S. Wen, and D. Tang, "Self-assembled topological insulator: Bi_2Se_3 membrane as a passive Q-switcher in an erbium–doped fiber laser," J. Lightwave Technol. **31**, 2857–2863 (2013).
126. Z. C. Luo, M. Liu, H. Liu, X. W. Zheng, A. P. Luo, C. J. Zhao, H. Zhang, S. C. Wen, and W. C. Xu, "2 GHz passively harmonic mode-locked fiber laser by a microfiber-based topological insulator saturable absorber," Opt. Lett. **38**, 5212–5215 (2013).
127. P. Tang, X. Zhang, C. Zhao, Y. Wang, H. Zhang, D. Shen, S. Wen, D. Tang, and D. Fan, "Topological insulator: Bi_2Te_3 saturable absorber for the passive Q-switching operation of an in-band pumped 1645-nm Er:YAG ceramic laser," IEEE J. Photon. **5**, 1500707 (2013).
128. M. Jung, J. Lee, J. Koo, J. Park, Y. W. Song, K. Lee, S. Lee, and J. H. Lee, "A femtosecond pulse fiber laser at 1935 nm using a bulk-structured Bi_2Te_3 topological insulator," Opt. Express **22**, 7865–7874 (2014).
129. Z. Q. Luo, C. Liu, Y. Z. Huang, D. D. Wu, J. Y. Wu, H. Y. Xu, Z. P. Cai, Z. Q. Lin, L. P. Sun, and J. Weng, "Topological-insulator passively Q-switched double-clad fiber laser at 2 μm wavelength," IEEE J. Sel. Top. Quantum Electron. **20**, 0902708 (2014).